Effect of random surface orientation on W sputtering yields

Jussila, J.

2018-12

Jussila , J , Granberg , F & Nordlund , K 2018 , ' Effect of random surface orientation on W sputtering yields ' , Nuclear Materials and Energy , vol. 17 , pp. 113-122 . https://doi.org/10.1016/j.nme.2018.08.002

http://hdl.handle.net/10138/250558
https://doi.org/10.1016/j.nme.2018.08.002

Nuclear Materials and Energy 17 (2018) 113–122

Contents lists available at ScienceDirect

Nuclear Materials and Energy

journal homepage: www.elsevier.com/locate/nme

Effect of random surface orientation on W sputtering yields

J. Jussila, F. Granberg*, K. Nordlund

Department of Physics, P.O. Box 43, FIN-00014 University of Helsinki, Finland

ARTICLE INFO

Keywords:
Sputtering
Tungsten
Irradiation
Helium
Argon

ABSTRACT

In this study, we investigate the sputtering yield of tungsten surfaces by energetic particles, focusing on the effect of surface orientation and the incoming irradiation angle, by means of molecular dynamics. We develop a simulation approach to simulate sputtering from completely random surface orientations. This allows obtaining the sputtering yields averaged over a sufficiently large number of orientations, to obtain statistically significant yields representative of a polycrystalline sample with random grain orientations. We find that the total sputtering yield is dependent on the surface orientation, and that the results for random surfaces are clearly different from that of any of the low-index ones or their average. The different low index surfaces and the random surfaces also showed that the sputtering yield is dependent on the incoming angle of the ion. The outgoing angle of the sputtered tungsten atoms was observed to be very sensitive to the surface orientation. Different features on the tungsten surface were observed to drastically affect the sputtering yield at certain angles.

1. Introduction

Fusion power is one of the most promising concepts for power generation in the future, and could be a feasible way to produce electricity on a large scale. There are, on the other hand, a lot of questions still unanswered and phenomena not yet fully understood. One important factor to be able to build the large power plants needed, are the plasma facing materials, as they need to withstand the damage produced by energetic particles. Several materials have been considered to be used as plasma facing components and as divertor material in fusion reactors [1–3], but the harsh conditions inside the reactor, like the heat and the irradiation, have shown to be challenging for any material [4–6]. For instance, if the melting point of the wall material is reached, the surface will melt and the particles and clusters molten away from the surface will cool down the plasma, and stop the nuclear reactions. Also, if the material cannot withstand the irradiation, the sputtering of surface atoms will cool down the plasma too much and stop the reaction, or may redeposit on other parts of the reactor wall, which would affect the operation. Tungsten is one of the materials of choice for fusion reactors under construction [1,2,7,8].

The sputtering yield of tungsten surfaces has been subject to investigations previously, both experimentally and computationally [9–17]. Already since the middle of the 20th century, many investigations have been conducted on the sputtering of tungsten surfaces by energetic ions [9,10]. The sputtering yield for a wide range of incoming ion energies has been obtained. The sputtering yield has also been seen to depend heavily on the mass of the incoming ion [11]. More recently, computer simulations have been carried out to investigate the sputtering yield. Many studies have been conducted on both pristine and modified surfaces, for instance He implanted ones [15,16]. Most studies, both experimental and computational, have, however, been conducted on perpendicular irradiation of the surface. Some studies have been done with different incoming angles of the ion, but they have, as most others also, focused on some low index tungsten surfaces [12–14]. In Ref. [18], simulations of W sputtering were carried out over random surfaces, however, no comparison with low-index ones and neither any studies of the effect of the incoming angle, were presented.

All structural materials manufactured for large scale practical applications will due to cost reasons be polycrystalline, and therefore the surface will have many random orientations. Hence, only considering the low index ones is not representative enough. The charged particles will hit the tungsten surfaces at both perpendicular as well as at random angles, depending on which part of the reactor we are looking at, as well as neutrals that can hit the surfaces at completely random angles [19]. It has also been seen that helium irradiation of tungsten surfaces can create tungsten fuzz [20–22], which will further roughen the surface and effectively change the incoming angle of the particles. Furthermore, experiments on roughened surfaces have shown that the features can drastically affect the reflection yield. For instance at high incoming angles, there is a high probability for reflection from a smooth surface, but for a rough surface, there is a higher probability for

* Corresponding author.
E-mail address: fredric.granberg@helsinki.fi (F. Granberg).

https://doi.org/10.1016/j.nme.2018.08.002
Received 24 January 2018; Received in revised form 3 August 2018; Accepted 3 August 2018

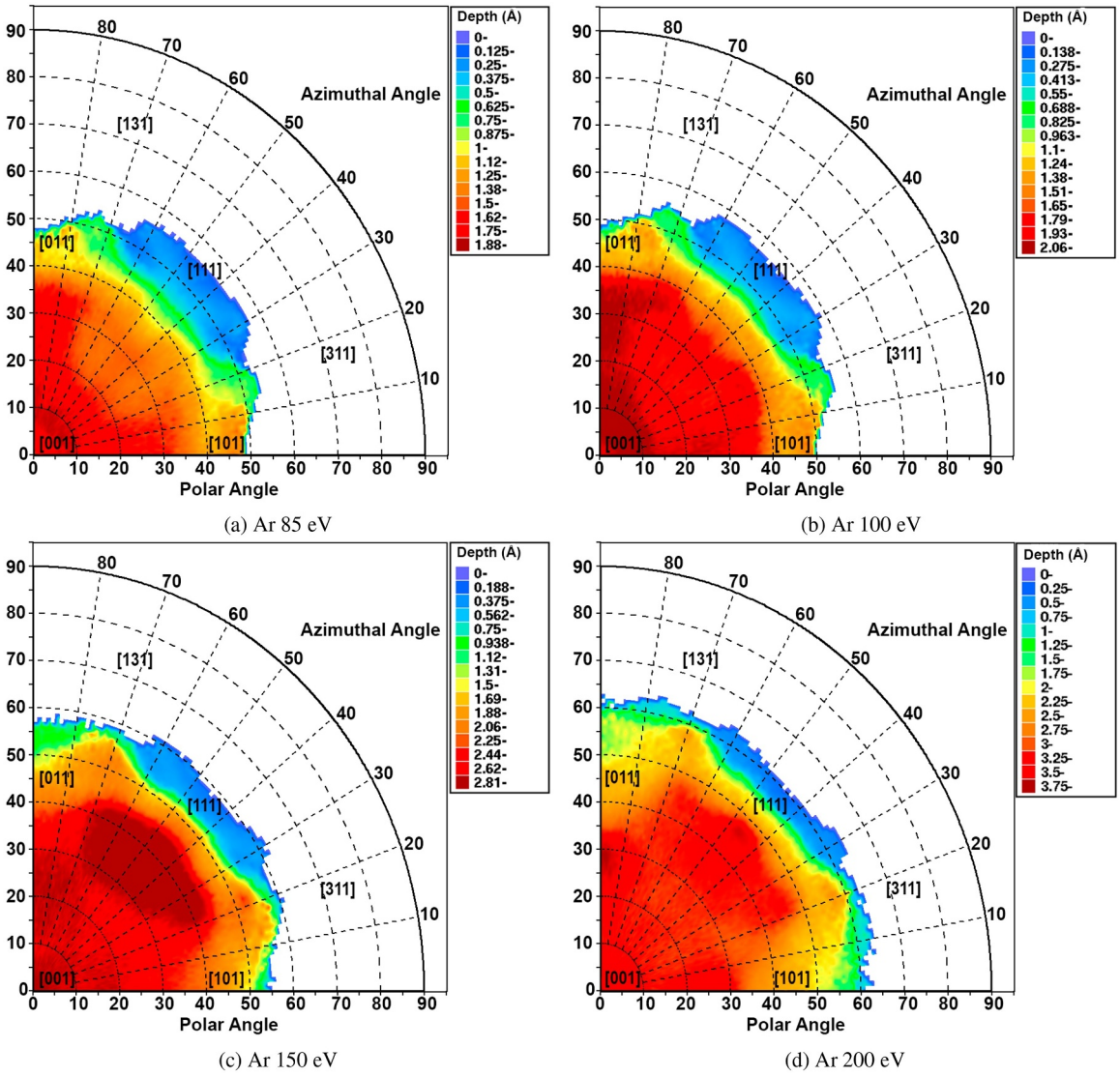

Fig. 1. W channeling maps for Ar irradiation. To make the color scale selection consistent, for each energy case, the minimum and maximum range for polar angles below 55° was found, and these values were used as the minimum and maximum of the color scale.

impact [23]. Especially the effect of random surface orientation has not been investigated thoroughly previously. Here, we study the effect of energetic particles hitting random surfaces at different angles and study the effect of both factors. We investigate the light element helium at four different energies and the heavier argon also at four different energies, to obtain the sputtering yield of tungsten of random surface orientation at different incoming angles. Fifty random tungsten surfaces are investigated at all incoming angles and the results are compared to low index surfaces, in our case the (001), (011) and (111) surfaces. The channeling maps of tungsten for the investigated elemental irradiations are also calculated and correlated to the obtained sputtering yields.

2. Methods

2.1. Channeling maps

We obtained maps showing the degree of channeling for all crystal directions following the procedure introduced in Ref. [24]. Briefly, molecular dynamics range calculations in the recoil interaction approximation were used to obtain the mean range for any given incoming ion direction (θ, ϕ). The θ and ϕ values were scanned at 1-degree intervals from 0 to 89° and 0 to 90°, respectively. In the W crystal, which has cubic symmetry, this is sufficient to obtain a picture of the channeling over all nonequivalent crystal directions. To correspond to a typical experimental situation of ions incoming on a surface, the range calculations are run allowing for ion reflection from the surface. Directions in which all 3000 incoming ions were reflected do not give any meaningful mean range, and hence are left blank in the channeling map plots.

2.2. Creating random surfaces

To simulate the sputtering yield of a randomly oriented W surface, we formed random surfaces using the following method, as previously also used in Ref. [18]. First, we created a tungsten cube and rotated it randomly using randomly selected Euler angles α_E, β_E and γ_E. The W cube had a body-centered cubic structure, with a lattice constant a corresponding to 300 K in the Marinica et al. potential [25], a_{300K} = 3.152 Å. The angle β_E was weighted by $\cos^{-1}(2u - 1)$ to correctly account for the randomness in 3D (u is a random number between 0 and 1).

A hemisphere with the radius, r_s, of 35 Å was cut out of the rotated cube and it was simulated in three different radial layers. A region from the center of the hemisphere to $r_s - 10$ Å was simulated in the NVE

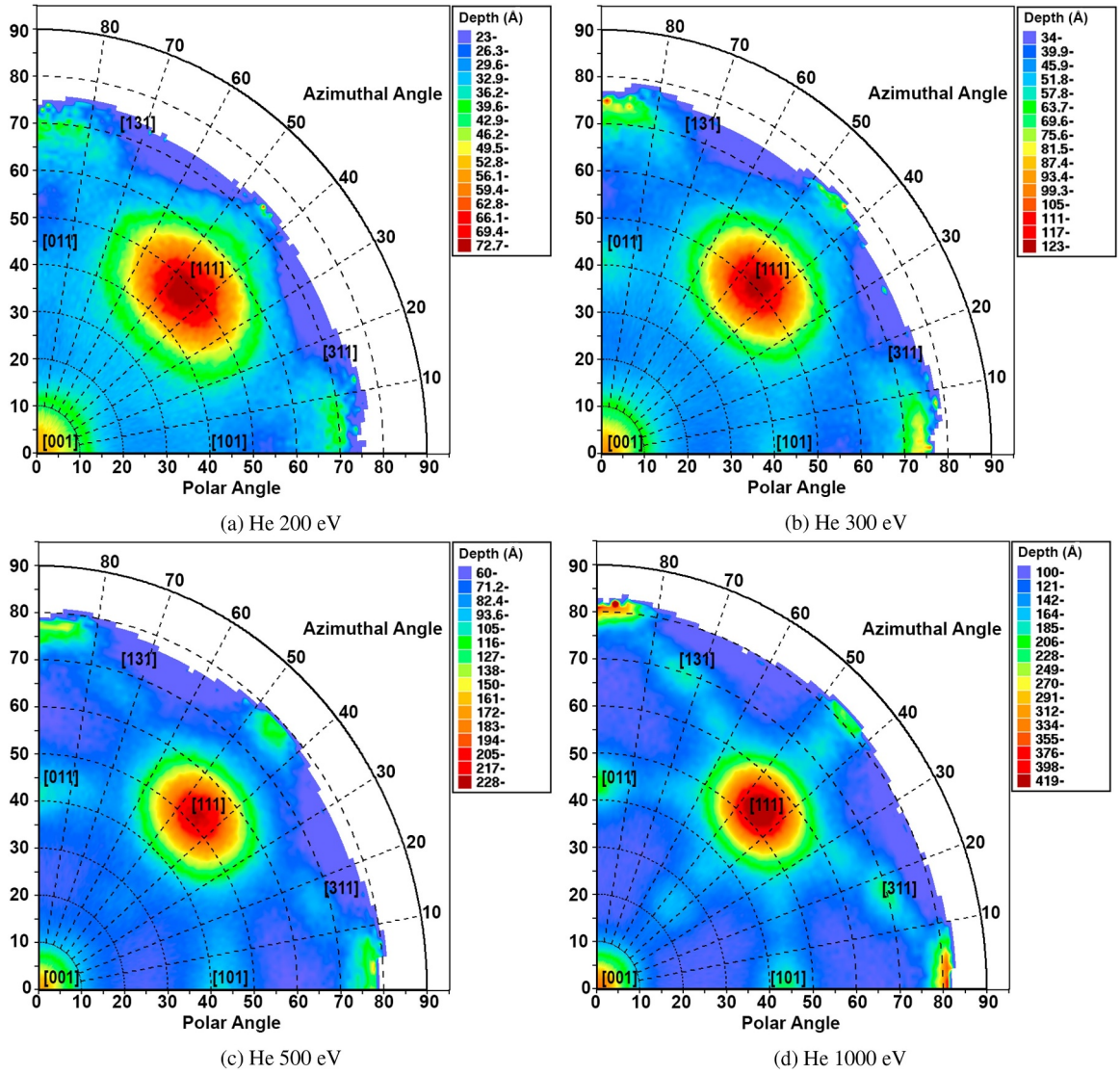

Fig. 2. W channeling maps for He irradiation. To make the color scale selection consistent, for each energy case, the minimum and maximum range for polar angles below 55° was found, and these values were used as the minimum and maximum of the color scale.

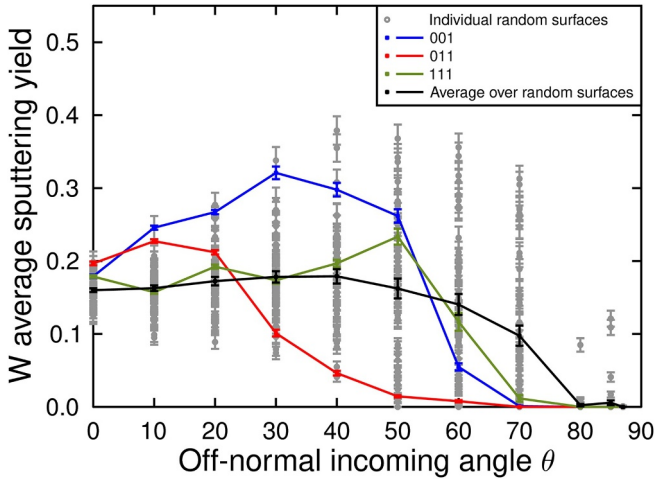

Fig. 3. Variation in sputtering yield of 100 eV Ar irradiation.

ensemble, to correctly handle many-body collisions caused by the incoming ion. In the middle region [r_s − 10 Å , r_s − 3 Å], the temperature of the atoms was scaled with a Berendsen thermostat [26], to keep the temperature constant due to the fixed atoms and to absorb the extra heat added to the system by the kinetic energy of irradiating ions. In the outermost region [r_s − 3 Å , r_s], the W atoms were fixed to prevent the cell from moving. After the creation of the randomly rotated cell, it was first simulated once at 300 K for 10 ps without any ion bombardment to relax the surface and to thermalize the cell.

2.3. Irradiation simulations

In our simulations we used two different elements, as the irradiating particles. Argon was chosen for its higher weight and helium for its light weight and for its relevancy to fusion energy production. Ar and He bombardments were initialized by placing the ion 7 Å above the surface of the hemisphere. Ions were chosen to hit in a random position inside a square bombardment area, which was located at the center of the hemisphere. The edge length of the bombardment area was 4a. To hit inside the bombardment area with different incoming angles θ, the initial positions of the ions were corrected compared to perpendicular bombardment. The incoming angle θ is defined compared to the

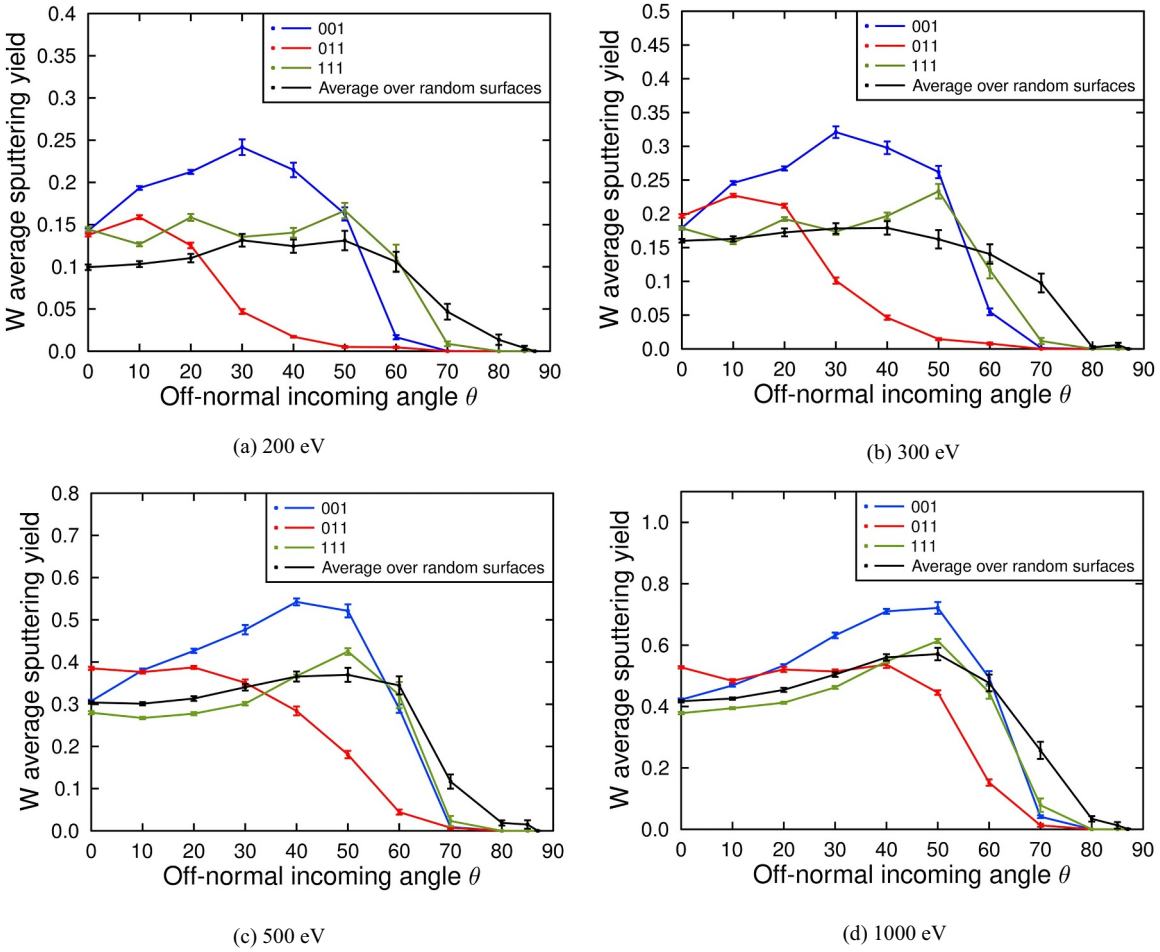

(a) 200 eV

(b) 300 eV

(c) 500 eV

(d) 1000 eV

Fig. 4. Average W sputtering yield for Ar irradiation.

perpendicular direction of the tungsten surface.

A total of 1000 incoming ions were simulated for each randomly oriented surface and every ion was irradiating a pristine surface. This bombardment was repeated for 50 different randomly generated surfaces for each energy and incoming angle. Same bombardments were also done for 30 different (001), (011) and (111) surfaces, where only the azimuthal direction of the surface was randomly chosen. These were constructed and relaxed in the same manner as the random surfaces. Sputtering yields were simulated for 11 different incoming angles θ and 4 + 4 different bombardment energies, depending on the ion. The incoming angles were 0°, 10°, 20°, 30°, 40°, 50°, 60°, 70°, 80°, 85°, 87°, Ar energies 85 eV, 100 eV, 150 eV and 200 eV, and He energies 200 eV, 300 eV, 500 eV and 1000 eV.

Simulations were carried out using the molecular dynamics code PARCAS [27]. We used the Marinica et al. potential with the modifications by Sand et al. [28] for interactions between W atoms, the Nordlund et al. [34] DMol potential between Ar and W atoms and the ZBL potential [29] between He and W atoms. Electronic stopping was ignored in Ar irradiations as the energies were low, but factored in for He irradiations. The electronic stopping was implemented as a friction force on all atoms with a kinetic energy of 10 eV or more, following common practise in the ion beam field [30–32].

Channeling maps, see Figs. 1 and 2, show that the mean range of He ions (Fig. 2) varies from 60 Å to 400 Å in the channeling directions, depending on energy. Because the radius of our simulation hemisphere is only 35 Å, many He ions pass through the hemisphere. It is possible that the He ion collides with fixed W atoms at the bottom of the hemisphere and bounces back through the surface of the hemisphere, giving unphysical reflection yields. To determine the fraction of such events, the exact trajectories of the ions were followed. We determined the number of ions reaching the fixed atom layers that were reflected. In the W sputtering calculations, it is not possible to determine if the sputtering of W atoms happened at the initial impact of the He ion or after He ion bounced back from the fixed bottom layer of the hemisphere. Hence, the average values of sputtering yields are calculated from all simulations, including those where the ion bounced from the fixed atom layer. The upper limit of the error is the standard error of the mean of all simulations. The lower limit of the error is adjusted to the worst-case scenario, where all the W sputtering happens after the He ions have bounced from the fixed layer. In the He reflection yield graphs, we excluded all the cases, where He ion contacted with the fixed layer. As the channeling maps show, preventing these collisions from happening would require to simulate He impacts correctly to depths of 400 Å, and this is beyond the computational resources available for this study. Corresponding simulations for a hemisphere radius of 50 Å were carried out for two incoming angles and two energies for the (001) surface. These results are presented in the supplementary material and showed to be in-line with the hemisphere radius of 35 Å simulations.

2.4. Analysis

To analyze W sputtering yields and Ar and He reflection yields, we used two different methods. The first method is a simple cutoff procedure. Every W atom or ion (Ar or He), whose position is 5.5 Å (the cutoff of the potential) above the surface of the hemisphere at the end of the simulation, is counted as a sputtered or reflected atom. The other method is based on cluster analysis and is able to identify, whether W

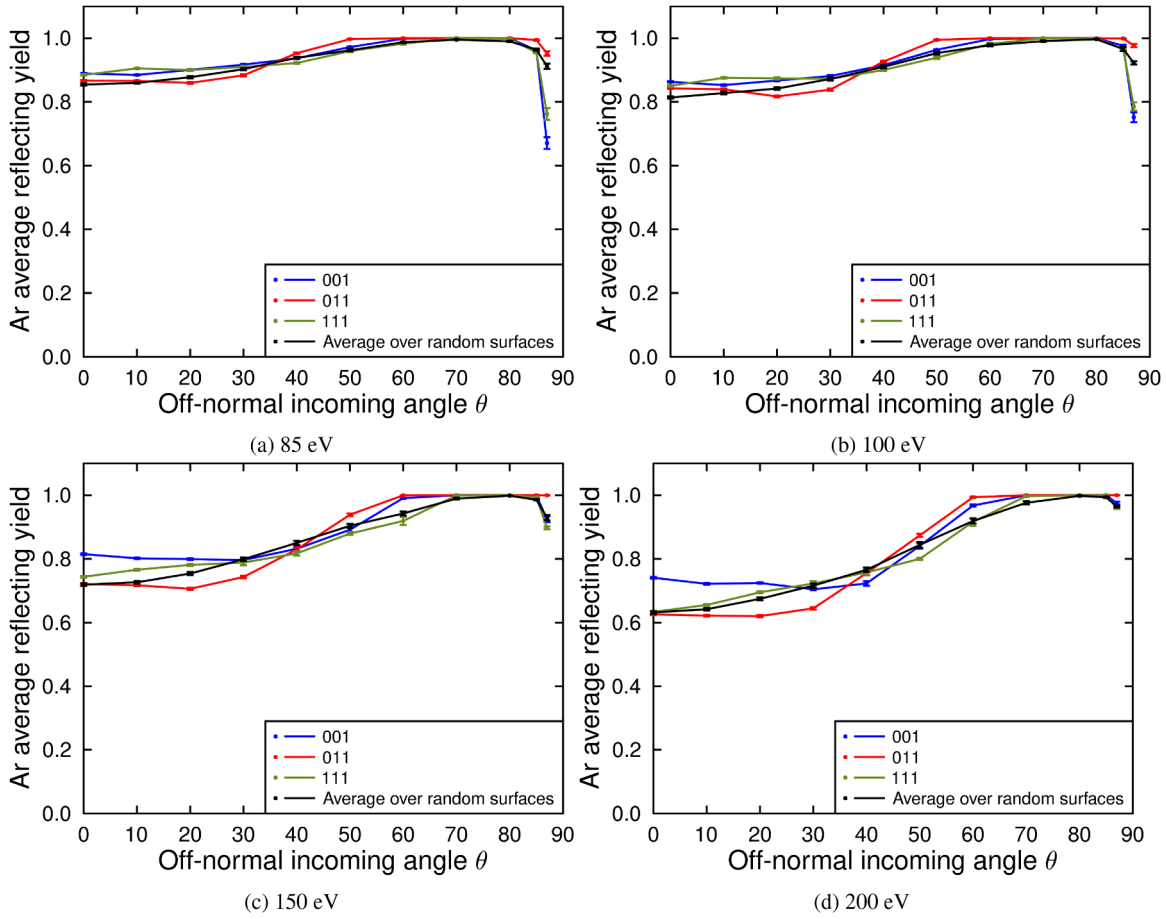

Fig. 5. Average Ar reflection yield for Ar irradiation. The apparent reduction in the reflection yield above 80° at the lower energies is related to the analysis approach, see text for details.

atoms have formed a protrusion on the surface, and accounted for that. In our simulations, we did not see a difference between the two methods as the energy of incoming projectiles is too low to form major W protrusions and craters on the surface. In some cases for Ar, at the highest incoming angles and the lowest energies, some of the reflected ions did not go over the cutoff, even though they left the hemisphere. These are not considered reflected in the present setup. This is because if the surface would be infinite, these ions would still have an interaction with the surface, and therefore react with it. Similarly, tungsten atoms leaving the surface, but not going over the cutoff are not considered sputtered, as they would also feel the attraction to the surface.

We collected data from both incoming and outgoing angular dependencies of sputtering and reflection yields. The average sputtering and reflection yields are plotted as a function of the incoming angle θ from zero to 87°. Data of the sputtering yield distribution of different outgoing angles of the ion were also studied. The outgoing angle α is measured the same way as the incoming angle θ. There is an individual outgoing sputtering and reflection yield distribution graph for every incoming angle and energy. In these graphs, the sputtering and reflection yields are plotted as a function of outgoing angle from zero to 90°.

In every graph, the error of the average surface is calculated as the standard error of the mean of single surface sputtering yields. We denote the sputtering yield of the surface i as x_i and the average sputtering yield of all N surfaces as $\bar{x}$. The standard error of the mean σ_x is calculated as:

$$\sigma_x = \frac{\sqrt{\sum_{i=1}^{N} \frac{1}{N}(\bar{x} - x_i)^2}}{\sqrt{N}}$$

3. Results and discussion

3.1. Channeling maps

The channeling maps for argon and helium irradiation of tungsten surfaces at different energies are presented in Figs. 1 and 2, respectively. In the channeling map of Ar, Fig. 1, we do not see a huge difference between the energies investigated. Noteworthy is that the mean range in the deepest channeling directions is only a few Ångströms, for Ar ions. In the channeling maps of He, Fig. 2, we also see a similar trend between the investigated energies. In contrast to the channeling maps of Ar, there are certain clear channeling directions for He, for instance the [001] and [111] directions, whereas the [011] is not a channeling direction. The mean ranges in the channeling directions are also much higher for He, on the scale of hundreds of Ångströms.

3.2. Effect of random surface

To examine the impact of random surface orientations, the average sputtering and reflection yields as a function of incoming angle θ for (001), (011), (111) and random surfaces are presented. In all graphs, the random surface is an average of 50 randomly rotated surfaces. Similarly, low index surfaces are an average of 30 corresponding index surfaces, which are rotated randomly only in an azimuthal direction. The sputtering and reflection yields per outgoing angular interval for all incoming angles and energies, can be found in the Supplementary material online.

We first discuss the magnitude of the variation of individual surfaces for the example case of 100 eV Ar on W. Fig. 3 shows the results for all

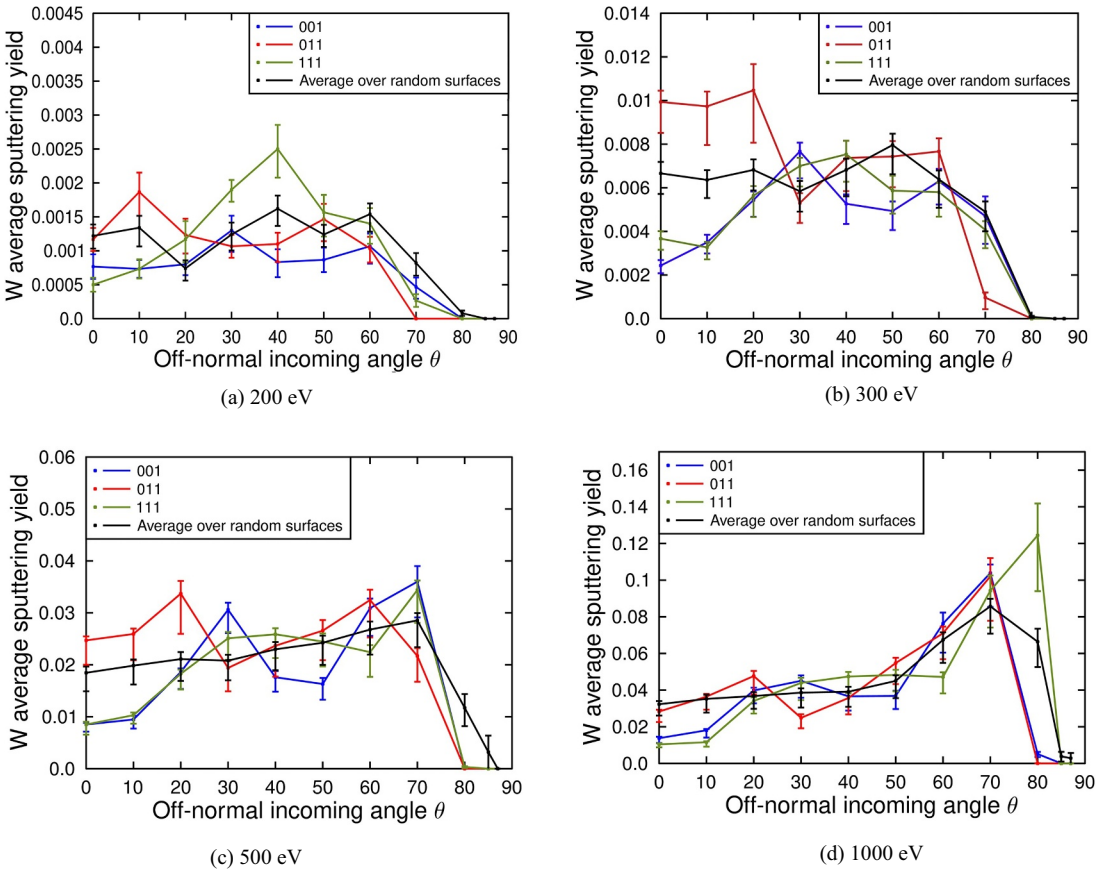

Fig. 6. Average W sputtering yield for He irradiation.

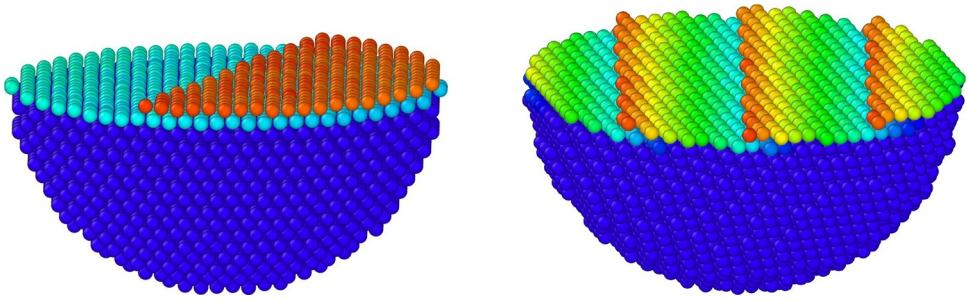

Fig. 7. Examples of surfaces where high sputtering yields were seen for high energy He bombardments.

50 individual surfaces in gray, their average in black, and the low-index surfaces (001), (011) and (111) in coloured lines. The results show that there are major variations in the results for different randomly oriented surfaces. Moreover, the average over the 3 low-index surfaces clearly would not become the same as the average over the random surfaces. The same observation is on a general level valid for almost all the cases studied in this paper, and the reasons to this difference are discussed in some detail below for several cases. For clarity in the plotting, in most of the remaining plots the results for individual random oriented surfaces are left out of the plots.

The average W sputtering yields for 85 eV, 100 eV, 150 eV and 200 eV Ar irradiation are plotted in Fig. 4. We notice that the surface orientation affects strongly the W sputtering yields at 85 eV and 100 eV energies. The effect is most significant for incoming angles between 20° and 60°. Simultaneously, the sputtering yield of the random surface is almost a constant in the same interval for the 85 eV bombardment. At low energies, we also see a clear separation between incoming angles, where the sputtering yield of each surface approaches zero. For 200 eV Ar bombardment, the relative differences between the sputtering yields of different surfaces are significantly smaller. Especially the sputtering yield profile of the (011) surface moves closer to the others. Similarly the incoming angle, where the sputtering yield approaches zero, shifts closer together. In all cases the overall shape of the graphs are similar. The sputtering yield of the (011) surface is the first and the averaged random surface is the last to approach zero at all energies. Interestingly, the sputtering yield of the averaged random surface is clearly lower than the low index surface sputtering yields at small incoming angles at 85 eV. However, this phenomenon does not occur at other energies. A sudden disappearance of (001) surface sputtering yield after incoming angles 50° at 85 eV and 60° at 200 eV is directly comparable with a channeling map Fig. 1(a) and (d). The 85 eV channeling map shows that the mean range of Ar projectiles is zero after 50°. This is also seen in the reflection yield graphs, as all incoming Ar ions will be reflected after the corresponding incoming angles.

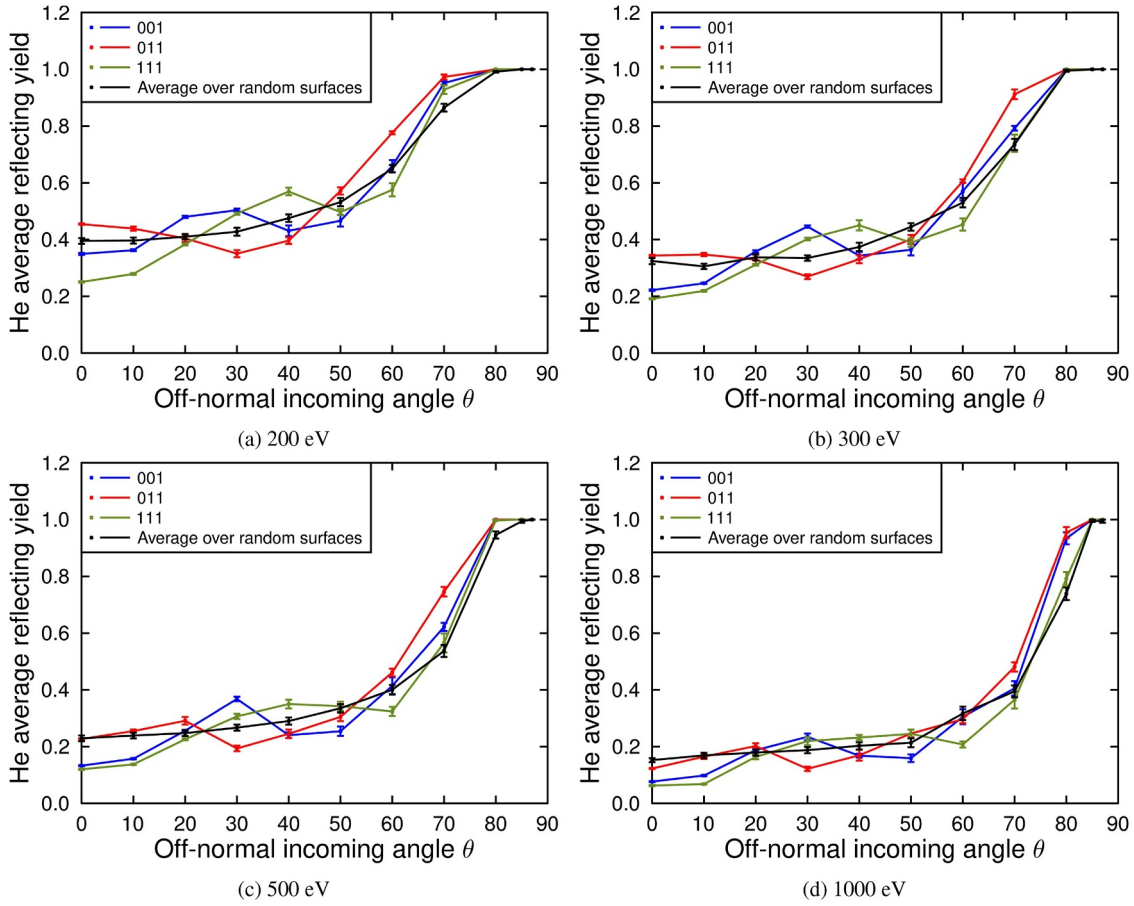

Fig. 8. Average He reflection yield for He irradiation.

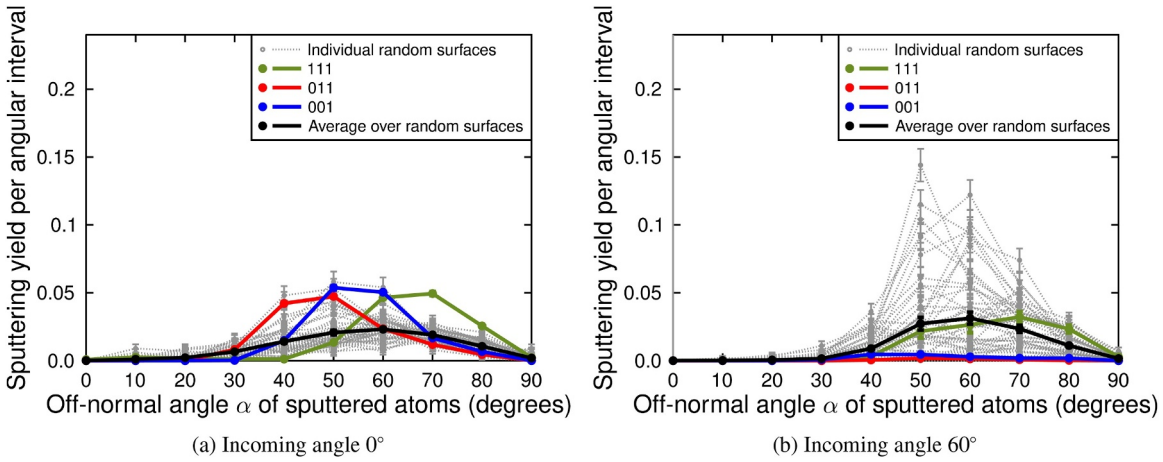

Fig. 9. Outgoing angular distribution of sputtered W atoms for 85 eV Ar irradiation.

The reflection yields of Ar for the same simulations are shown in Fig. 5. In the case of 85 eV and 100 eV, reflection yields of low index surfaces are nearly identical to the reflection yield of the averaged random surfaces. Because of the low energy of the incoming ion, there is not much variation in reflection yield due to different incoming angles. Only for the highest incoming angles and the lower recoil energies the reflection yields of the surfaces drop considerably. This do not indicate that the ion did not reflect, but that the end position was not over the cutoff of the potential. For the incoming angles 70° and 80° we see that almost all ions are reflected and almost none trapped in the sample. The latter holds true also for the incoming angles 85° and 87°, where almost none of the ions are retained in the sample, but ions are not considered sputtered due to the cutoff criterion. This should also be taken into account when looking at the reflection yield per angular interval, as the reflected atoms not over the cutoff are not included. For higher energies, differences between surface orientations start to form. We see a clear growth of reflection yield for all surfaces, when the incoming angle grows. For 200 eV perpendicular bombardment $\theta = 0°$, reflection yield of (001) surface is higher than random, (011) or (111) surface reflection yields. According to the Ar 200 eV channeling map,

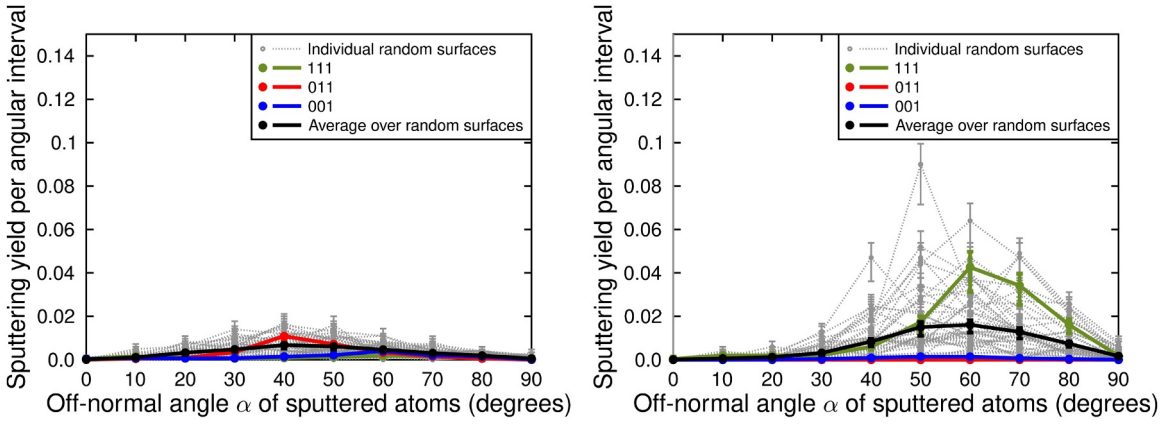

(a) Incoming angle 0° (b) Incoming angle 80°

Fig. 10. Outgoing angular distribution of sputtered W atoms for 1000 eV He irradiation.

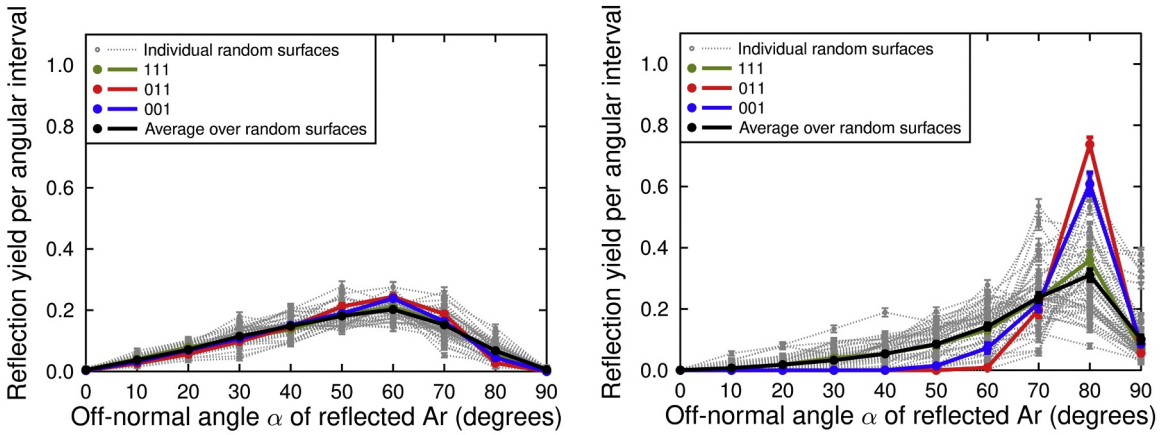

(a) Incoming angle 60° (b) Incoming angle 80°

Fig. 11. Outgoing angular distribution of reflected Ar ions for 85 eV Ar irradiation.

Fig. 1(d), the [001] direction is a stronger channeling direction than [011] or [111] directions, and therefore its reflection yield should be lower. This seems like a surprising result, because a similar behaviour does not happen in He bombardments. As seen in the Ar channeling map, the highest mean range in channeling directions is only a couple of Ångströms, which may cause the different behaviour, compared to hundreds in the case of He irradiation.

Tungsten sputtering yields for He irradiation at 200 eV, 300 eV, 500 eV and 1000 eV are illustrated in Fig. 6. In the case of 200 eV, W sputtering occurs very rarely (on average 1 sputtered atom per surface orientation) and large errors make it difficult to compare sputtering yields between different surfaces.

For perpendicular bombardment, the W sputtering yields of (001) and (111) surfaces are clearly lower than sputtering yields of (011) and random surfaces. This is seen at all energies, but the relative difference is largest for 300 eV ions. The 300 eV channeling map, Fig. 2(b), shows that [001] and [111] are channeling directions, but [011] is not. Therefore, the perpendicular bombardment into a channeling direction is linked to a lower W sputtering yield. For the 500 eV and 1000 eV simulations, the W sputtering yield of averaged random surfaces grows along the incoming angle θ, until θ reaches a collapse point of sputtering yield. For higher energy simulations, the collapse of the sputtering yield of the random surface occurs at a higher incoming angle and the sputtering yield drop is steeper. This includes all energies from 200 eV to 1000 eV. There is also a high peak around $\theta = 80°$ in the sputtering yield of (111) surface at 1000 eV.

An interesting detail of the 1000 eV He simulations is that the sputtering yield of the averaged random surfaces does not reach a zero value at $\theta = 87°$ or even at $\theta = 85°$. For all other energies, the random surface sputtering yield is zero at $\theta = 87°$. It turns out that there is only one random surface out of fifty, which has non-zero sputtering yield in the case of $\theta = 87°$ at 1000 eV. Sputtering yield of this single random surface is extremely high and it raises the average random surface sputtering yield apart from the zero value. Also at $\theta = 85°$ there are three non-zero sputtering yield surfaces, out of which two have a high and the third a negligible sputtering yield. A similar case also happens at the incoming angle $\theta = 85°$ at 500 eV bombardments. The shapes of these unusually high sputtering yield surfaces are illustrated in Fig. 7. The color coding refers to the height in the direction of the surface normal. From the figures we can see the edge in the center of the simulation cell, where the ions have their impact point. The tungsten atoms at this edge can easily, even at very large angles, be sputtered away from the surface. This shows the importance of simulating non-perfect non-low-index surfaces when investigating the sputtering yields of different surfaces.

The reflection yields of all above He simulations are plotted in Fig. 8. Every simulation is in agreement with the channeling maps (see Fig. 2) at an incoming angle $\theta = 0°$ bombardment. For all energies, (001) and (111) surfaces are strongest channeling directions and their reflection yields are the lowest in perpendicular bombardment. Therefore, a strong channeling direction indicates a lower reflection yield, and vice versa. The effect of channeling direction can be also seen from the (001) surface reflection yield changes as the incoming angle grows. The most significant drop in reflection yield for all energies happens

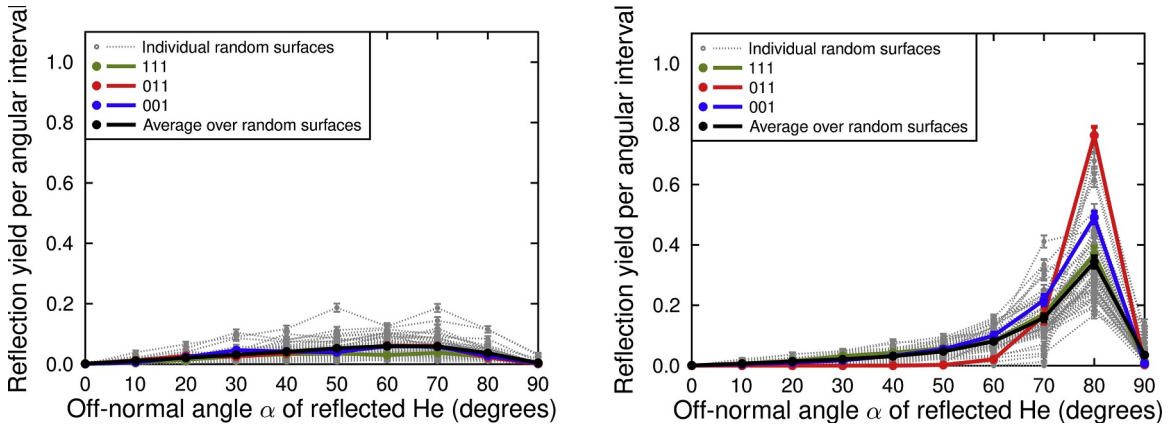

(a) Incoming angle 60°

(b) Incoming angle 80°

Fig. 12. Outgoing angular distribution of reflected He ions for 1000 eV He irradiation.

between incoming angles 40° and 50°. In the channeling maps, the average (001) bombardment simulation corresponds to an average mean range value with the same polar angle as the incoming angle of the irradiating ion. Therefore, the [111] channeling direction causes the drop of (001) surface reflection yield at those incoming angles. The drop can be also seen in He sputtering yield graphs, Fig. 6.

3.3. Variations in outgoing angle

To study the outgoing angular distribution of sputtered W atoms and reflected Ar or He ions, both yields were plotted as a function of the outgoing angle α. The angle α is measured in the same way as the incoming angle θ, the spherical coordinate from the normal of the W surface. Sputtered atoms are sorted in bins and the sputtering yields of the bins are expressed in the graphs. The 10° bin contains sputtered atoms whose outgoing angle is between 5° and 15°. The width of the first and the last bin is only 5°. An outgoing angle graph was produced for every energy and incoming angle. All graphs are included in the Supplementary material found online. As described in sections 2.4 and 3.2, atoms leaving the surface but not going over the cutoff are excluded from the results. In the analysis, we only focus on a few remarkable cases.

We notice from Fig. 9 that (001), (011) and (111) surfaces have nearly equal total sputtering yields in a perpendicular 85 eV Ar bombardment, but their outgoing angular sputtering yield distributions are shifted apart from each other. When the incoming angle is increased, total sputtering yields of different surfaces changes according to the incoming angle graphs. Every surface has its strongest outgoing sputtering directions in the same outgoing angle α for all incoming angles. The random surface has a wider outgoing angle spectrum than low index surfaces, but it does not have a clearly identifiable peak. The spread of the sputtering yields for a single random surface compared to the sputtering yield of the averaged surfaces is relatively small in the perpendicular bombardment (the individual random surface results are marked by light gray lines in the graphs). When the incoming angle reaches 50°, we begin to observe individual random surfaces with extremely high sputtering yields. Many times these surface have one dominant outgoing angle α. This phenomenon can be seen in Fig. 9(b). Overall the outgoing sputtering angle distribution for Ar 100 eV, 150 eV and 200 eV irradiations are very similar to the 85 eV Ar irradiation. Only the incoming angle, where single random surface sputtering yields start to differ from the averaged random surface sputtering yield, shifts to a higher value.

For 200 eV and 300 eV He simulations, errors in sputtered atoms outgoing angle distributions are too large to analyze the results meaningfully. There may be only one sputtered atom in a single outgoing angle bin. Outgoing angular distributions for incoming angles 0° and 80° for 1000 eV He irradiation are presented in the Fig. 10. For the perpendicular bombardment, the sputtering yield of every surface is lower than for larger incoming angles. Still, there are single random surfaces, which sputtering yields are many times larger than low index surfaces yields. The most dominant outgoing angles of low index surfaces are the same as in Ar simulations. However the incoming angle, where the single random surface sputtering yields starts to vary the most, is shifted to a θ value of 80°, which can be seen in Fig. 10(b).

The outgoing angular distribution of reflected Ar ions is very similar for all investigated energies. At small incoming angles, reflected Ar ions are rather evenly distributed between both sides of $\alpha = 40°$. There is only minimal difference between different low index surfaces and independent random surfaces. Fig. 11(a) shows that this still holds for the incoming angle 60° in 85 eV bombardment, even though the distribution has started to weight towards larger outgoing angles. When the incoming angle grows even more, a very sharp peak rapidly forms to an outgoing angle $\alpha = 80°$, seen in Fig. 11(b). Eventually nearly all Ar ions are reflected at over 60° outgoing angles. For all large incoming angles, the spread of sputtering yields of single random surfaces increases, and some random surfaces have very high reflective yields at small outgoing angles ($\alpha = 0° - 70°$).

The outgoing angular distribution of reflected He ions behaves the same way as Ar ions. Fig. 12 shows the outgoing angular dependency of reflected He ions with the same incoming angles as in the Ar graphs. The most distinct difference between Ar and He results is that there are less single random surfaces, whose outgoing sputtering yield distribution differs from the average random surface distribution.

4. Conclusions

We have studied the sputtering of tungsten surfaces under ion irradiation and focused of the effect of surface orientation. The effect of random surfaces was investigated and compared to commonly studied low index surfaces. We note that the current case of purely randomly selected surfaces may not exactly correspond to experimental samples, since the macroscopic processing methods may lead to a preference for lower index surfaces. Hence the current study should be considered the limiting case of a sample processed in such a way that the surface orientation is completely random. We found some similarities between the random surface and the others, but already between different low index surfaces there are differences in the magnitude of the sputtering yield. The average random surface at almost all energies has a sputtering yield between the low index surfaces at perpendicular or low incoming angle irradiation. For the higher incoming angles, especially the ones close to parallel to the surface we saw drastic changes. For

instance the averaged random surface always had higher sputtering yield than the low index surface for high incoming angles. Also in some cases the sputtering yield did not drop to 0, as for the other cases, which was explained by the features on the specific random surface. The low index surfaces, and their sputtering and reflective yield, could be directly compared to the channeling maps of the specific configuration, and clear correlations could be seen. We saw a decrease in both sputtering yield and reflective yield in the strongly channeling directions, compared to incoming angles close to the channel. The outgoing angle of both the sputtered tungsten atoms and the reflected ions was measured in angular intervals, which could be directly compared to experiments. This study showed a different profile for the different low index surfaces and also for the random one, where the low index surfaces usually showed a more defined peak, whereas the random surface showed a much broader peak.

Acknowledgments

This work has been carried out within the framework of the EUROfusion Consortium and has received funding from the Euratom research and training programme 2014–2018 under grant agreement No 633053. The views and opinions expressed herein do not necessarily reflect those of the European Commission.

Supplementary material

All the sputtering and reflection yields per angular interval, for all investigated energies, incoming angles and ions can be found in the Supplementary online material.

Supplementary material associated with this article can be found, in the online version, at 10.1016/j.nme.2018.08.002

References

[1] ITER Physics Basis Editors ITER Physics Expert Group Chairs and Co-Chairs and ITER Joint Central Team and Physics Integration Unit, ITER physics basis, Nucl. Fusion 39 (12) (1999) 2137–2638.
[2] Progress in the ITER Physics Basis editors, Progress in the ITER physics basis, Nucl. Fusion 47 (6) (2007) 1–413.
[3] J. Wesson, Tokamaks, Second, Oxford Engineering Series, Clarendon Press, Oxford, 1997.
[4] J. Knaster, A. Moeslang, T. Muroga, Materials research for fusion, Nat. Phys. 12 (2016) 424–434, https://doi.org/10.1038/nphys3735.
[5] V.P. Budaev, Results of high heat flux tests of tungsten divertor targets under plasma heat loads expected in ITER and tokamaks (review), Phys. Atomic Nuclei 79 (7) (2016) 1137–1162, https://doi.org/10.1134/S106377881607005X.
[6] Y. Ueda, J. Coenen, G.D. Temmerman, R. Doerner, J. Linke, V. Philipps, E. Tsitrone, Research status and issues of tungsten plasma facing materials for ITER and beyond, Fusion Eng. Design 89 (7) (2014) 901–906, https://doi.org/10.1016/j.fusengdes.2014.02.078.
[7] G. Janeschitz, Plasmawall interaction issues in ITER, J. Nucl. Mater. 290–293 (Supplement C) (2001) 1–11, https://doi.org/10.1016/S0022-3115(00)00623-1.
[8] H. Bolt, V. Barabash, W. Krauss, J. Linke, R. Neu, S. Suzuki, N. Yoshida, ASDEX Upgrade Team, Materials for the plasma-facing components of fusion reactors, J. Nucl. Mater. 329–333 (Part A) (2004) 66–73, https://doi.org/10.1016/j.jnucmat.2004.04.005.
[9] N. Matsunami, Y. Yamamura, Y. Itikawa, N. Itoh, Y. Kazumata, S. Miyagawa, K. Morita, R. Shimizu, H. Tawara, Energy dependence of the ion-induced sputtering yields of monatomic solids, At. Data Nucl. Data Tables 31 (1) (1984) 1–80, https://doi.org/10.1016/0092-640X(84)90016-0.
[10] Y. Yamamura, H. Tawara, Energy dependence of ion-induced sputtering yields from monoatomic solids at normal incidence, At. Data Nucl. Data Tables 62 (2) (1996) 149–253, https://doi.org/10.1006/adnd.1996.0005.
[11] G. Wehner, Influence of the angle of incidence on sputtering yields, J. Appl. Phys. 30 (11) (1959) 1762–1765, https://doi.org/10.1063/1.1735051.
[12] A. Azens, G. Romanovskis, U. Kanders, A molecular dynamics study of the sputtering of the W(100) surface by low-energy He, Ar and Kr ions, J. Phys. 4 (22) (1992) 5053, https://doi.org/10.1088/0953-8984/4/22/005.
[13] E. Salonen, K. Nordlund, J. Keinonen, C.H. Wu, Molecular dynamics studies of the sputtering of divertor materials, J. Nucl. Mater. 313–316 (Supplement C) (2003) 404–407, https://doi.org/10.1016/S0022-3115(02)01397-1.
[14] X. Yang, A. Hassanein, Molecular dynamics simulation of erosion and surface evolution of tungsten due to bombardment with deuterium and carbon in tokamak fusion environments, Nucl. Inst. Meth. Phys. Res. Sec. B 308 (Supplement C) (2013) 80–87, https://doi.org/10.1016/j.nimb.2013.05.012.
[15] F. Sefta, N. Juslin, K.D. Hammond, B.D. Wirth, Molecular dynamics simulations on the effect of sub-surface helium bubbles on the sputtering yield of tungsten, J. Nucl. Mater. 438 (Supplement) (2013) S493–S496, https://doi.org/10.1016/j.jnucmat.2013.01.101.
[16] F. Ferroni, K.D. Hammond, B.D. Wirth, Sputtering yields of pure and helium-implanted tungsten under fusion-relevant conditions calculated using molecular dynamics, J. Nucl. Mater. 458 (Supplement C) (2015) 419–424, https://doi.org/10.1016/j.jnucmat.2014.12.090.
[17] A. Lasa, C. Björkas, K. Vörtler, K. Nordlund, MD simulations of low energy deuterium irradiation on W, WC and W_2c surfaces, J. Nucl. Mater. 429 (2012) 284–292, https://doi.org/10.1016/j.jnucmat.2012.06.012.
[18] E. Marenkov, K. Nordlund, I. Sorokin, A. Eksaeva, K. Gutorov, J. Jussila, F. Granberg, D. Borodin, Angular and velocity distributions of tungsten sputtered by low energy argon ions, J. Nucl. Mater. 496 (2017) 18–23, https://doi.org/10.1016/j.jnucmat.2017.09.021.
[19] R. Behrisch, G. Federici, A. Kukushkin, D. Reiter, Material erosion at the vessel walls of future fusion devices, J. Nucl. Mater. 313–316 (Supplement C) (2003) 388–392, https://doi.org/10.1016/S0022-3115(02)01580-5.
[20] M.J. Baldwin, R.P. Doerner, Helium induced nanoscopic morphology on tungsten under fusion relevant plasma conditions, Nucl. Fusion 48 (3) (2008) 035001, https://doi.org/10.1088/0029-5515/48/3/035001.
[21] A. Lasa, K. Henriksson, K. Nordlund, MD simulations of onset of tungsten fuzz formation under helium irradiation, Nucl. Inst. Meth. Phys. Res. Sec. B 303 (Supplement C) (2013) 156–161, https://doi.org/10.1016/j.nimb.2012.11.029.
[22] A. Lasa, S.K. Tähtinen, K. Nordlund, Loop punching and bubble rupture causing surface roughening – a model for W fuzz growth, Europhys. Lett. 105 (2) (2014) 25002, https://doi.org/10.1209/0295-5075/105/25002.
[23] S. Brezinsek, A. Hakola, H. Greuner, M. Balden, A. Kallenbach, M. Oberkofler, G.D. Temmerman, D. Douai, A. Lahtinen, B. Bswirth, D. Brida, R. Caniello, D. Carralero, S. Elgeti, K. Krieger, H. Mayer, G. Meisl, S. Potzel, V. Rohde, B. Sieglin, A. Terra, R. Neu, C. Linsmeier, Surface modification of He pre-exposed tungsten samples by He plasma impact in the divertor manipulator of ASDEX upgrade, Nucl. Mater. Energ. 12 (2017) 575–581, https://doi.org/10.1016/j.nme.2016.11.002.
[24] K. Nordlund, F. Djurabekova, G. Hobler, Large fraction of crystal directions leads to ion channeling, Phys. Rev. B 94 (2016) 214109, https://doi.org/10.1103/PhysRevB.94.214109.
[25] M.C. Marinica, L. Ventelon, M.R. Gilbert, L. Proville, S.L. Dudarev, J. Marian, G. Bencteux, F. Willaime, Interatomic potentials for modelling radiation defects and dislocations in tungsten, J. Phys. 25 (39) (2013) 395502, https://doi.org/10.1088/0953-8984/25/39/395502.
[26] H.J.C. Berendsen, J.P.M. Postma, W.F. van Gunsteren, A. DiNola, J.R. Haak, Molecular dynamics with coupling to an external bath, J. Chem. Phys. 81 (8) (1984) 3684–3690, https://doi.org/10.1063/1.448118.
[27] K. Nordlund, 2010, PARCAS computer code. The main principles of the molecular dynamics algorithms are presented in [31,33]. The adaptive time step and electronic stopping algorithms are the same as in [30].
[28] A.E. Sand, J. Dequeker, C.S. Becquart, C. Domain, K. Nordlund, Non-equilibrium properties of interatomic potentials in cascade simulations in tungsten, J. Nucl. Mater. 470 (2016) 119–127, https://doi.org/10.1016/j.jnucmat.2015.12.012.
[29] J.F. Ziegler, J.P. Biersack, U. Littmark, The Stopping and Range of Ions in Matter, Pergamon, New York, 1985.
[30] K. Nordlund, Molecular dynamics simulation of ion ranges in the 1–100 keV energy range, Comput. Mater. Sci. 3 (1995) 448, https://doi.org/10.1016/0927-0256(94)00085-Q.
[31] K. Nordlund, M. Ghaly, R.S. Averback, M. Caturla, T. Diaz de la Rubia, J. Tarus, Defect production in collision cascades in elemental semiconductors and FCC metals, Phys. Rev. B 57 (13) (1998) 7556–7570, https://doi.org/10.1103/PhysRevB.57.7556.
[32] A. Tamm, G. Samolyuk, A.A. Correa, M. Klintenberg, A. Aabloo, A. Caro, Electron-phonon interaction within classical molecular dynamics, Phys. Rev. B 94 (2016) 024305, https://doi.org/10.1103/PhysRevB.94.024305.
[33] M. Ghaly, K. Nordlund, R.S. Averback, Molecular dynamics investigations of surface damage produced by keV self-bombardment of solids, Phil. Mag. A 79 (4) (1999) 795, https://doi.org/10.1080/01418619908210332.
[34] K. Nordlund, N. Runeberg, D. Sundholm, Repulsive interatomic potentials calculated using Hartree-Fock and density-functional theory methods, Nucl. Instrum. Methods Phys. Res. B 132 (1) (1997) 45–54, https://doi.org/10.1016/S0168-583X(97)00447-3.